12th International Symposium on Turbulence and Shear Flow Phenomena (TSFP12)
Osaka, Japan (Online), July 19-22, 2022

STOCHASTIC MODELING OF THREE-SCALAR MIXING IN A COAXIAL JET USING ONE-DIMENSIONAL TURBULENCE

Marten Klein
Lehrstuhl Numerische Strömungs- und Gasdynamik
Brandenburgische Technische Universität
Siemens-Halske-Ring 15A
D-03046 Cottbus, Germany
marten.klein@b-tu.de

Christian Zenker
Fachgebiet Numerische Mathematik und Wissenschaftliches Rechnen
Brandenburgische Technische Universität
Platz der Deutschen Einheit 1
D-03046 Cottbus, Germany
christian.zenker@b-tu.de

Tommy Starick
Lehrstuhl Numerische Strömungs- und Gasdynamik
Brandenburgische Technische Universität
Siemens-Halske-Ring 15A
D-03046 Cottbus, Germany
tommy.starick@b-tu.de

Heiko Schmidt
Lehrstuhl Numerische Strömungs- und Gasdynamik
Brandenburgische Technische Universität
Siemens-Halske-Ring 15A
D-03046 Cottbus, Germany
heiko.schmidt@b-tu.de

ABSTRACT

Modeling complex mixing processes is a standing challenge for a number of applications ranging from chemical to mechanical and environmental engineering. Here, the gas-phase turbulent mixing in a three-stream concentric coaxial jet is investigated as a canonical problem. Reynolds-averaged Navier–Stokes simulations (RANS) suggest that the gas-phase mixing can be accurately modeled by air doped with passive scalars, for which small-scale resolving numerical simulations are performed with the one-dimensional turbulence (ODT) model as stand-alone tool. We show that both the spatial (S-ODT) and temporal (T-ODT) model formulations yield qualitatively similar results exhibiting reasonable to good agreement with available reference experiments, Reynolds-averaged and large-eddy simulations, as well as mixing models. This is demonstrated for low-order statistics, like the scalar variance and dissipation, but also the two-scalar joint probability density functions that can not be obtained with RANS. Our results suggest that S-ODT has better capabilities than T-ODT to model the mixing processes in the jet which we attribute to the account of local advective time scales.

INTRODUCTION

Turbulent mixing denotes the filamentation and diffusion of conserved flow variables on a range of scales in a chaotic, notionally random flow field. Filamentation occurs due to reversible stirring motions, whereas molecular diffusion is irreversible by nature. While direct numerical simulation (DNS) resolves all relevant scales of the flow directly, it is often far to expensive for extrapolation to parameter regimes relevant to applications. Conventional turbulence models used in Reynolds-averaged Navier–Stokes simulation (RANS) and large-eddy simulation (LES) aim to overcome this bottleneck by treating turbulent mixing as a continuous, irreversible mixing process. Such models are, therefore, of limited applicability for flows with complex mixing and possibly active scalars with multiphysicale small-scale processes.

Taking chemically-reacting jets as a relevant application, it is well known that the location and maximum of the heat release in a non-premixed jet flame crucially depends on the hydrodynamic mixing of chemical species prior to combustion (e.g. Pitsch & Steiner (2000); Echekki *et al.* (2001); Cabra *et al.* (2005); Walter *et al.* (2015)). In order to better understand the mixing process, a single passive scalar has been investigated for various settings (e.g. Dowling & Dimotakis (1990); Klein *et al.* (2019)). Albeit the relevant scales have been resolved by these experimental and numerical approaches, cross-correlations and differential diffusion effects between different chemical species were not captured. Therefore, multiscalar mixing has been investigated recently (e.g. Giddey *et al.* (2018); Li *et al.* (2021)). A feasible and canonical application case is the three-stream mixing (e.g. Cai *et al.* (2011)) or, equivalently, two-conserved-scalar mixing (e.g. Rowinski & Pope (2013)), in a coaxial round jet that is considered here.

In this study, we address the standing numerical challenges associated with the high-fidelity representation of multiple scalar mixing in a concentric coaxial round jet (see figure 1) by utilizing the lower-order stochastic one-dimensional turbulence (ODT) model (Kerstein (1999)) as stand-alone tool. Here, we apply and compare the temporal and spatial model formulations for cylindrical geometry (Lignell *et al.* (2018)). We demonstrate that ODT is able to capture scalar joint probability density functions of the multiscalar mixing but also discuss its shortcomings.

Below, we briefly describe the configuration, the modeling approach, and the simulation set-up. After that, we discuss the mixing by comparing ODT to RANS and available reference data. Last, we give some concluding remarks.

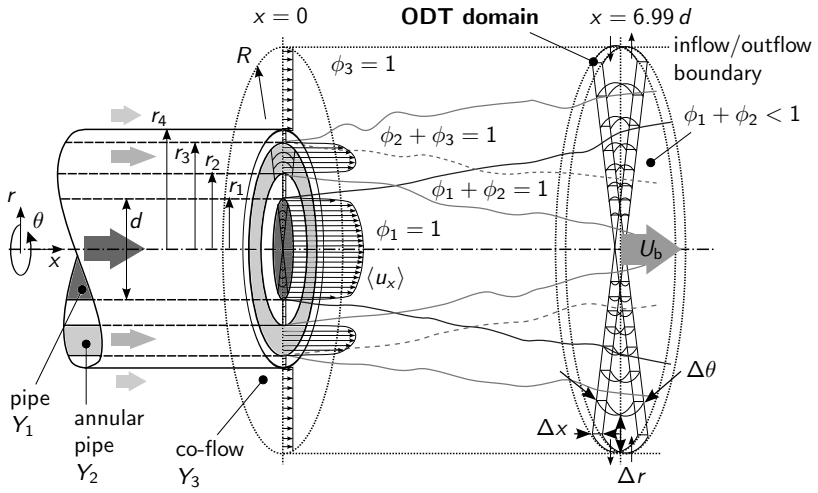

Figure 1. Sketch of the three-stream coaxial jet configuration investigated. A round and a concentric coaxial annular jet issue into a slow co-flow at downstream location $x/d = 0$ with the sketched mean velocity profile $\langle u_x \rangle(r)$ due to walls at radial locations r_1–r_4. The domain boundary is located at $R \gg r_4$. The inflow streams $i = 1,2,3$ contain different passive scalars with initially uniform mass fraction Y_i or mixture fraction ϕ_i, respectively. The ODT domain is a two-sided infinitesimal wedge that spans the diameter and is advected downstream with bulk velocity U_b. See table 1 for further details.

A THREE-STREAM COAXIAL JET

Figure 1 shows a sketch of the cylindrical three-stream configuration. The mixing of a central round and a concentric coaxial annular jet surrounded by a slower co-flow is investigated downstream of a three-stream nozzle. The set-up is comparable to that of Cai *et al.* (2011), who experimentally investigated the mixing of an inner acetone-doped jet of air with an annular ethylene jet and co-flow air. The inflow streams are gases with mass fraction Y_i ($i = 1,2,3$) and mixture fraction $\phi_i = Y_i/(Y_1 + Y_2 + Y_3)$. Following Rowinski & Pope (2013) and Dowling & Dimotakis (1990) for gas-phase concentration mixing, we simplify the configuration to three inflow streams of air with homogeneous kinematic viscosity ν and mass density ρ. Every stream is doped with a different passive scalar of diffusivity Γ_i as detailed below and in table 1. Here, two low-fidelity RANS simulation cases have been considered, one replicating the experimental inflow streams and the other treating gas-phase concentrations as passive scalars. The results are virtually indistinguishable (in agreement with Dowling & Dimotakis (1990)) so that we adopt the case of passive scalar for our ODT and RANS simulations shown below.

The coaxial jet is characterized by the jet Reynolds numbers $Re_1 = U_{\mathrm{b},1}\, r_1/\nu = 7130$ and $Re_2 = U_{\mathrm{b},2}\,(r_3 - r_2)/\nu = 3974$ that are based on the bulk velocity $U_{\mathrm{b},i}$ in each inflow stream in between the positive radial intervals $[0, r_1]$ and $[r_2, r_3]$. The co-flow is uniform and laminar in $[r_4, R]$. The gas-phase composition is characterized by the concentration diffusivity relative to air. This is expressed for the two jets by the Schmidt numbers $Sc_1 = \nu/\Gamma_1 = 1.29$ and $Sc_2 = \nu/\Gamma_2 = 0.565$. Note that the scalar in the co-flow has zero diffusivity ($\Gamma_3 = 0$). This scalar only labels the co-flow air, which does not diffuse in itself. However, we keep track of its advection since turbulent entrainment of co-flow fluid affects the mixture fractions ϕ_i downstream of the nozzle.

Table 1. Details of the inflow streams $i = 1,2,3$ in figure 1. Nominal reference values (ref) are based on Cai *et al.* (2011).

property	central jet	annular jet	co-flow
i	1	2	3
$r_{\mathrm{inner},i}$ [mm]	—	3.175	4.75
$r_{\mathrm{outer},i}$ [mm]	2.77	4.19	75
$U_{\mathrm{b},i}$ [m/s]	34.5	32.5	0.4
$\rho_{\mathrm{ref},i}$ [kg/m^3]	1.26	1.14	1.17
$\nu_{\mathrm{ref},i}$ [mm^2/s]	13.4	8.3	15.9
$\rho_i = \rho$ [kg/m^3]	1.168	1.168	1.168
$\nu_i = \nu$ [mm^2/s]	15.9	15.9	15.9
Γ_i [mm^2/s]	10.39	14.69	0

MODEL OVERVIEW AND SIMULATION SET-UP

Modeling The Mean State Using RANS

Computational fluid dynamics has become a powerful tool in analyzing engineering problems over the last decades. An established approach is RANS in which the Reynolds-averaged Navier–Stokes and scalar conservation equations are solved by modeling the mean effects of unresolved fluctuations with the aid of the Boussinesq closure assumptions. Here, 3-D RANS equations have been solved numerically using Ansys® Academic Research CFD, Release 2021 R2. The computational domain is $100d$ long and contains an inflow section of length $20d$ such that fully-developed pipe and annular pipe flows exit the nozzle at $x = 0$. No-slip zero-scalar-flux boundary conditions are prescribed at the radial walls, except for $r = R$, which is treated as free-slip wall. Inflow and outflow boundary conditions are prescribed in axial direction. The grid contains $\approx 5 \times 10^7$ cells with local refinement at the nozzle walls and across the conical influence region of the jet. A conventional k–ω shear-stress transport (SST) closure model with default model parameters is used that can handle wall-attached and free-stream turbulence. The main purpose of the present RANS analysis is to assess the simplification to passive scalar mixing and to provide additional low-fidelity reference data.

The differences between gas-phase and passive scalar mixing are marginal so that we limit our attention to the latter case.

Stochastic Modeling Using ODT

The key idea of the one-dimensional turbulence (ODT) model (Kerstein (1999)) is to resolve the flow on all relevant scales, but only for a notional line-of-sight. Deterministic processes (like molecular diffusion) are directly resolved along the lower-order computational domain, whereas turbulence is modeled by a stochastically-sampled sequence of discrete eddy events with momentary rate $\tau^{-1} = C\sqrt{2E/l^2}$, where C is the eddy rate parameter, l the eddy size, and E the specific available eddy energy. E is obtained based on the momentary flow state as $E = E_{\text{kin}} - ZE_{\text{vp}}$, where $E_{\text{kin}} = u_{x,K}^2$ and $E_{\text{vp}} = \nu^2/l^2$ denote the kinetic and viscous penalty contributions, respectively. $u_{x,K}$ is a kernel-weighted eddy scale velocity and Z the small-scale suppression parameter.

Eddy events punctuate the deterministic flow evolution by application of a conservative (measure-preserving) map that instantaneously modifies flow profiles by a permutation of fluid elements along the 1-D domain. Eddy events are characterized by three random variables: the eddy size, radial location, and time (or axial location) of occurrence. Energetically plausible ($E > 0$) candidate events are considered for probabilistic acceptance if an eddy turnover fits into the elapsed simulation time, that is, $\tau \leq \beta_{\text{LS}} t$ for T-ODT or with t by inversion of $x(t)$ for S-ODT, where β_{LS} is the large-scale suppression parameter (Echekki *et al.* (2001)).

For the round jet sketched in figure 1, the ODT domain is an infinitesimal double-wedge that spans the diameter and has open boundaries in the co-flow region. The two subdomains for positive and negative radial (r) locations are coupled by a symmetric center cell in order to minimize flux imbalances due the the coordinate singularity at the axis within the stand-alone model (Lignell *et al.* (2018)). The ODT domain is advected downstream with bulk velocity U_{b} during a simulation run, which is done a differently in the temporal (T-ODT) and spatial (S-ODT) model formulations (Kerstein (1999)).

In T-ODT, the ODT domain is interpreted as a closed system and lower-order conservation equations are formulated for the physically conserved quantities. Synthetic flow profiles are resolved along the radius r and evolve in time t during a simulation run while the entire ODT domain is uniformly displaced in axial direction as $x(t) = \int_0^t U_{\text{b}}(t')\,\mathrm{d}t'$, where $U_{\text{b}}(t)$ is radially uniform. Following Echekki *et al.* (2001); Klein *et al.* (2019), but taking into account the cylindrical geometry (Starick *et al.* (2019)), $U_{\text{b}} = U_3 + \int_{-R}^{R} \rho(u-U_3)^2 r\,\mathrm{d}r \Big/ \int_{-R}^{R} \rho(u-U_3) r\,\mathrm{d}r$. The elliptic flow problem is, hence, approximated by a parabolized set of conservation equations. Here, we assume a minimal model and resolve only the axial velocity component u_x together with the scalar mass fractions Y_i ($i = 1,2,3$) such that

$$\frac{\partial u_x}{\partial t} + \text{eddies} = \frac{1}{r}\frac{\partial}{\partial r}\left(\nu r \frac{\partial u_x}{\partial r}\right) - \frac{1}{\rho}\frac{\mathrm{d}P}{\mathrm{d}x}, \tag{1}$$

$$\frac{\partial Y_i}{\partial t} + \text{eddies} = \frac{1}{r}\frac{\partial}{\partial r}\left(\Gamma_i r \frac{\partial Y_i}{\partial r}\right), \tag{2}$$

where the mean pressure gradient $\mathrm{d}P/\mathrm{d}x$ is only used for the generation of turbulent inflow conditions as described below. An eddy event is implemented by an instantaneous mapping that moves fluid from location $f(r)$ to mapped location r such that $u_x(r) \to u_x\big(f(r)\big)$ and $Y_i(r) \to Y_i\big(f(r)\big)$. A shortcoming of T-ODT is that it can not capture induced radial momentum fluxes since the continuity equation is not part of the model. This deficiency is partly compensated by the domain displacement $x(t)$ mentioned above, but, strictly, T-ODT is applicable only to flows that are statistically invariant in downstream and spanwise direction such as channel or pipe flows.

In S-ODT, a local time-to-space transformation is used (Kerstein (1999)). In the adaptive formulation (Lignell *et al.* (2018)), grid cells are displaced with their local axial velocity $u_x(r,x)$. Hence, for a fixed spatial increment δ_x, molecular diffusion has more time to take effect where u_x is low. The ratio of the local advective ($\delta_x/u_x(r)$) to the diffusive (δ_x^2/ν, δ_x^2/Γ_i) time scales is more accurately represented in S-ODT than T-ODT. S-ODT avoids the ambiguity with respect to downstream advection but it requires $u_x(r) > 0$. The S-ODT equations specialized to round jets read

$$\frac{\partial u_x u_x}{\partial x} + \frac{1}{r}\frac{\partial r u_r u_x}{\partial r} + \text{eddies} = \frac{1}{r}\frac{\partial}{\partial r}\left(\nu r \frac{\partial u_x}{\partial r}\right), \tag{3}$$

$$\frac{\partial u_x Y_i}{\partial x} + \frac{1}{r}\frac{\partial r u_r Y_i}{\partial r} + \text{eddies} = \frac{1}{r}\frac{\partial}{\partial r}\left(\Gamma_i r \frac{\partial Y_i}{\partial r}\right). \tag{4}$$

It is worth noting that the radial velocity u_r is *not* resolved directly but induced by the application of physical conservation laws whenever needed. This is done separately for the deterministic advancement and eddy implementations. In the algorithm, $u_r \neq 0$ manifests itself by radial displacements of the Lagrangian grid cell interfaces such that the axial mass and momentum flux is conserved for each Lagrangian cell.

For further technical details, the reader is deferred to Lignell *et al.* (2018). Following their notation, we utilize the triplet map TMA with eddy-rate evaluation for the radial coordinate. A symmetric center cell of size $\Delta r_{\text{axis}} = 0.15\,\text{mm}$ is used which is by a factor 10 larger (factor 2 smaller) than the smallest (largest) allowed grid cell size to ensure coupling of the subdomains with $r \gtrless 0$. Grid adaption is performed upon triplet map implementation and enforced after two diffusive advancement steps independent of eddy event occurrences. The ODT model parameters have been estimated by pre-simulations with a small ensemble yielding $C = 5$, $Z = 400$, and $\beta_{\text{LS}} = 3.5$ for S-ODT (all similar to Lignell *et al.* (2018)), whereas $\beta_{\text{LS}} = 0.4$ for T-ODT (as in Echekki *et al.* (2001); Klein *et al.* (2019)). These parameters are kept constant for the jet simulations shown below.

Generation Of Inflow Conditions

Figure 2 shows low-order statistics and an instantaneous ODT radial profile of the axial velocity at the nozzle exit. For RANS, jet inflow conditions are obtained by extending the simulated flow domain with nozzle walls to negative x. There, initially uniform flow profiles are prescribed that develop towards the statistically steady-state and exit the nozzle at $x/d = 0$. For ODT, we follow the self-consistent procedure described in Klein *et al.* (2019). Mean profiles are consistent with our but differ from the reference RANS. T-ODT simulations of pipe ($C = 5$, $Z = 350$, maximum eddy size $l_{\max} = 2r_1/3$) and annular pipe ($C = 10$, $Z = 600$, $l_{\max} = 2(r_3 - r_2)/3$) flows are therefore conducted as pre-simulations. A large number of flow profiles is sampled from the statistically steady state of both internal flows in order to generate an $N = 50{,}000$ ensemble of perturbed inflow profiles from each of which an independent ODT jet simulation was started after adding the co-flow and the scalar to the inflow streams. For S-ODT, the inflow condition has been regularized by truncation of $u_x(r,0)$ with $u_{x,\min} = U_3/2$ across the wall regions $[r_1, r_2]$ and $[r_3, r_4]$.

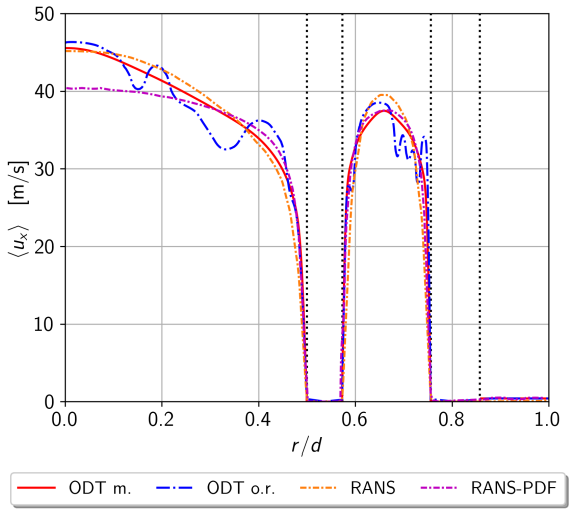

Figure 2. Radial profiles of the axial velocity at $x/d = 0$ across $0 \leq r/d \leq 1$. Mean (m.) and instantaneous (one realization, o. r.) profiles from ODT, RANS, and reference RANS (RANS-PDF, Rowinski & Pope (2013)) are shown.

RESULTS

Flow Visualization

Figure 3 shows axial-radial snapshots of the jet colored by the scalar mixture fraction ϕ_2 from the annular region for our RANS and an S-ODT realization demonstrating that ODT is capable of capturing the mean state. A T-ODT realization (not shown) gives qualitatively similar results. ODT thus provides a synthetic flow solution that aims to be statistically representative in terms of mean but contains additional information on the large and small scale fluctuations.

Low-Order Scalar Statistics At The Axis

Figure 4 shows downstream profiles of the ensemble mean $\langle \phi_i \rangle$ and variance $\langle \phi_i'^2 \rangle$, where $\phi_i' = \phi_i - \langle \phi_i \rangle$, for the scalar mixture fractions ϕ_1 and ϕ_2, respectively, for T-ODT, S-ODT, our RANS, and reference experiments. RANS is unable to fully capture the axial mean profiles in contrast to ODT, which agrees with experiments capturing the potential core ($x/d \lesssim 5$), the local fluctuation maximum (within $7 < x/d < 9$), and the decay. S-ODT predicts a two times larger variance maximum. This behavior is likely singular due to strongly fluctuating axial velocities which may be different for finite radial distances addressed below.

Radial Profiles Of Low-Order Scalar Statistics

Figure 5 shows radial profiles of the mean $\langle \phi_i \rangle$ and fluctuation variance $\langle \phi_i'^2 \rangle$ of the scalar mixture fraction ϕ_i, $i = 1,2$, for T-ODT, S-ODT, our RANS, and reference experiments form Cai *et al.* (2011) for $x/d = 6.99$. ODT results are consistent with RANS for the mean but all three models do not reproduce low-order statistical moments in the outer region ($r/d > 1.2$). In the vicinity of the axis ($r/d < 0.4$), T-ODT exhibits physically more reasonable fluctuation variances than S-ODT as it does not take into account local advection time scales. Correspondingly, only S-ODT accurately captures fluctuations across the shear region ($0.4 < r/d < 1.2$) in which the complex mixing takes place.

Joint Probability Density Function

Figure 6 shows two-scalar joint probability density functions (JPDFs) for T-ODT (top row) and S-ODT (bottom row) in terms of the mixture fractions ϕ_1 and ϕ_2 for radial locations $r/d = 0.387, 0.635, 0.992$, but fixed axial location $x/d = 6.99$. Detailed S-ODT statistics are well within the 99 percentile of the reference experiments from Cai *et al.* (2011) satisfactorily reproducing the shape and mean state at all points across the shear region of the three-stream annular jet. The JPDFs obtained with T-ODT are degraded which is reminiscent of multiscalar mixing in isotropic turbulence (Giddey *et al.* (2018)). The T-ODT mean state is consistent with RANS but the agreement of the JPDF is reasonable only for $r/d = 0.635$. The bulk velocity U_b is 20.8 m/s (18.0 m/s) for S-ODT (T-ODT) and reached at $r/d = 0.660$ (0.520). The ensemble-averaged axial velocity profile $\langle u_x \rangle(r)$ (not shown here) is monotonically decreasing with $r > 0$ for $x > 4d$, so local advection time scales at $r/d = 0.387$ (0.992) are smaller (larger) than that associated with the uniform U_b. This explains why S-ODT captures the complex mixing better than T-ODT.

Dissipation Of Scalar Fluctuations

Figure 7 shows the dissipation rate of the scalar fluctuation variance $\langle \chi_i \rangle = \sum_{j=1}^{3} 2\Gamma_i \langle (\partial \phi_i / \partial x_j)^2 \rangle$ for $i = 1,2$ which is a relevant measure for micromixing and an important quantity for the evaluation of mixing-model fidelity as it is related to mixing time scales. In ODT, the dissipation rate is approximated as $\langle \chi_i \rangle \approx 2\Gamma_i \langle (\partial \phi_i / \partial r)^2 \rangle$. Present results indicate that only S-ODT is able to yield dissipation rates $\langle \chi_1 \rangle$ and $\langle \chi_2 \rangle$ that are close to the reference experiments and a RANS-PDF (IEM) method. T-ODT simulations, by contrast, fail to capture $\langle \chi_2 \rangle$. Diffusive closure models as those used in the reference LES (or stand-alone RANS) likewise tend to overestimate the dissipation of scalar fluctuations.

CONCLUSION

Small-scale resolving numerical simulations of the turbulent mixing of passive scalars in a three-stream concentric coaxial jet using RANS and the one-dimensional turbulence (ODT) model as stand-alone tool. Both the temporal (T-ODT) and spatial (S-ODT) model formulations for cylindrical geometry give qualitatively similar results that are consistent with RANS for the mean state and capture details of available reference data. For the spatially developing jet, S-ODT is preferred as it more accurately captures details of the complex mixing such as the joint probability density function and the dissipation of scalar fluctuations. This property can be attributed to the model formulation, since S-ODT aims to capture the ratio of local advective and diffusive time scales. Based on the present study, ODT can be more confidentially applied to multiphysical mixing in free shear flows like reactive jets or wakes that require small-scale fidelity. Forthcoming research will build upon the detailed representation of scalar and momentum mixing by utilizing ODT as autonomous microscale model within a bottom-up LES approach (Kerstein (2022)).

REFERENCES

Cabra, R., Chen, J.-Y., Dibble, R. W., Karpetis, A. N. & Barlow, R. S. 2005 Lifted methane–air jet flames in a vitiated coflow. *Combust. Flame* **143**, 491–506.

Cai, J., Dinger, M. J., Li, W., Carter, C. D., Ryan, M. D. & Tong, C. 2011 Experimental study of three-scalar mixing in a turbulent coaxial jet. *J. Fluid Mech.* **685**, 495–531.

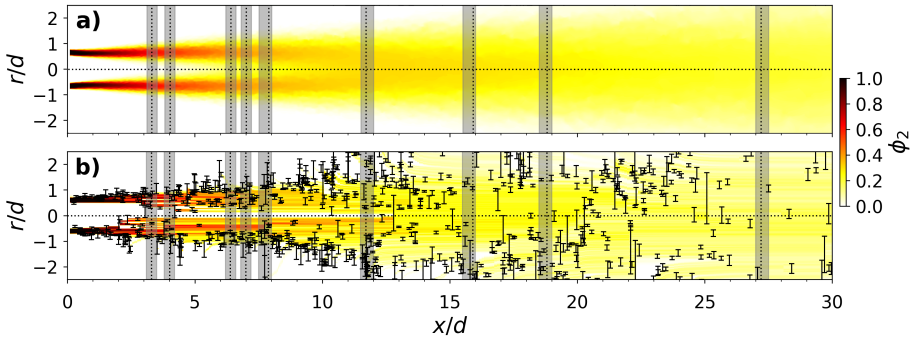

Figure 3. Radially and axially truncated axial-radial section of the jet showing the pseudo-colored mixture fraction ϕ_2 for our RANS (a) and one S-ODT realization (b). Black vertical lines with caps denote discrete eddy events. Gray regions and dotted lines are used for detailed comparison with available reference data.

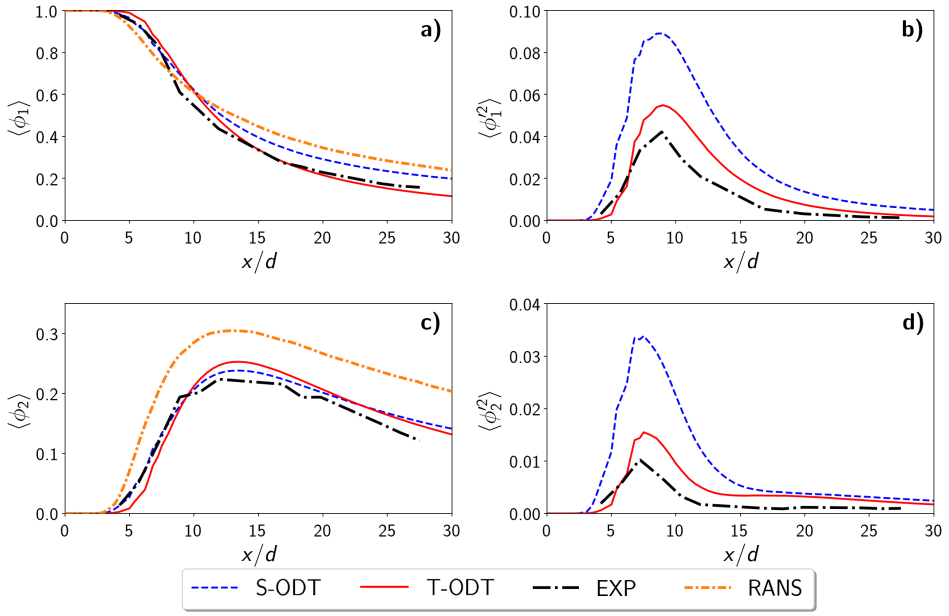

Figure 4. Downstream profiles of low-order scalar statistics at the jet axis ($r/d = 0$) for our RANS, ODT, and reference experiments (EXP) from Cai *et al.* (2011) showing the mean (a, c) and fluctuation variance (b, d) of the scalar mixture fractions ϕ_1 and ϕ_2.

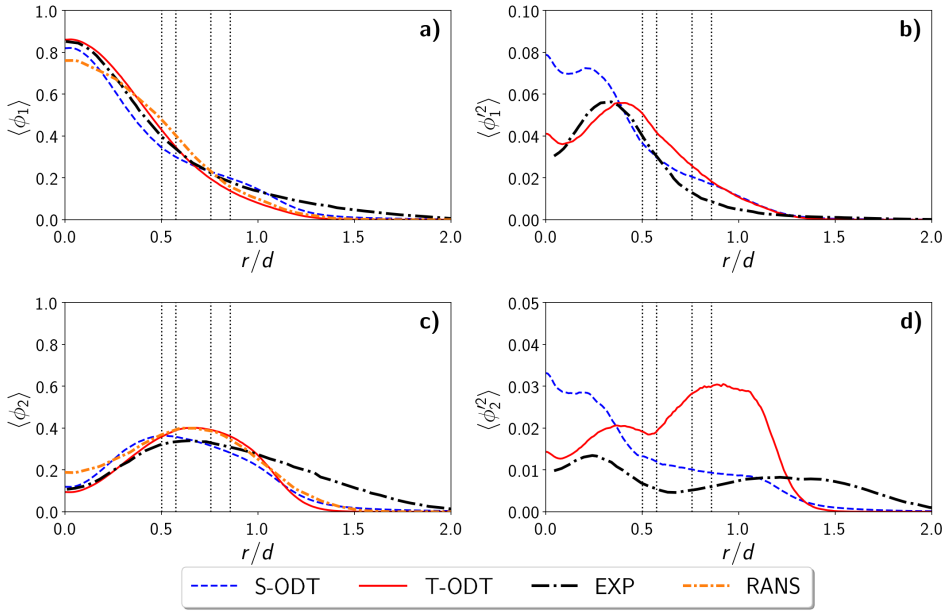

Figure 5. Radial profiles of low-order scalar statistics at $x/d = 6.99$ for our RANS, ODT, and reference experiments (EXP). Labels and line styles are the same as in figure 4. In addition, vertical lines give the locations r_1–r_4 of the nozzle walls for orientation.

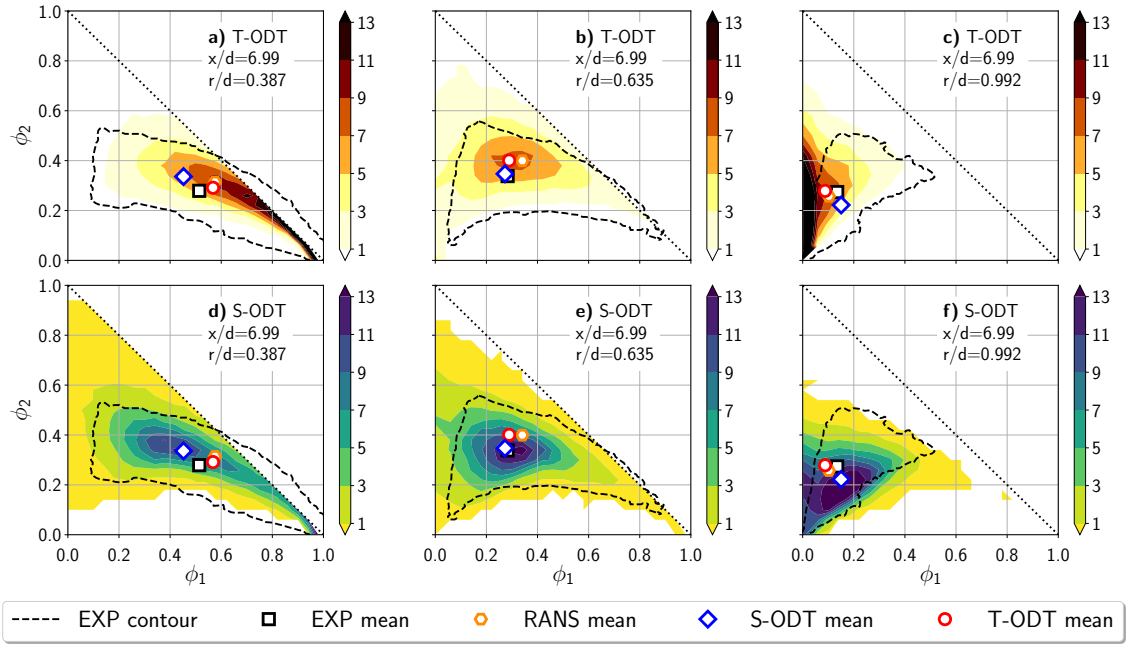

Figure 6. Scalar joint probability density functions (JPDFs) for mixture fractions ϕ_1 and ϕ_2 at downstream location $x/d = 6.99$ and radial locations $r/d = 0.387$ (a, d), $r/d = 0.635$ (b, e), and $r/d = 0.992$ (c, f) from $N = 50{,}000$ ODT realizations. Different color scales visually distinguish T-ODT (a–c) from S-ODT (d–f). The dashed contour gives the 99 percentile of the experimentally measured JPDF (Cai *et al.* (2011)). Open symbols denote the mean states for ODT, experiments, and our RANS. The area above the diagonal is inaccessible for passive scalars in constant-density flow.

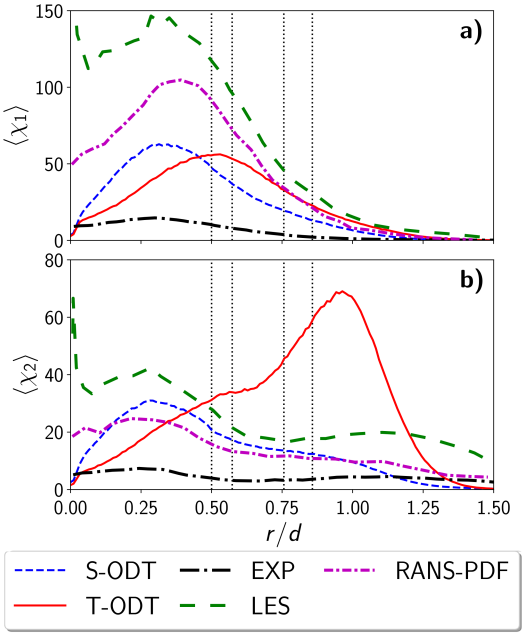

Figure 7. Radial profiles of the dissipation rates $\langle\chi_1\rangle$ (a) and $\langle\chi_2\rangle$ (b) of the scalar fluctuation variance at $x/d = 6.99$. Reference experiments are from Cai *et al.* (2011). RANS-PDF and LES reference results are from Rowinski & Pope (2013).

Dowling, D. R. & Dimotakis, P. E. 1990 Similarity of the concentration field of gas-phase turbulent jets. *J. Fluid Mech.* **218**, 109–141.

Echekki, T., Kerstein, A. R., Dreeben, T. D. & Chen, J.-Y. 2001 'One-dimensional turbulence' simulation of turbulent jet diffusion flames: Model formulation and illustrative applications. *Combust. Flame* **125**, 1083–1105.

Giddey, V., Meyer, D. W. & Jenny, P. 2018 Modeling three-dimensional scalar mixing with forced one-dimensional turbulence. *Phys. Fluids* **30**, 125103.

Kerstein, A. R. 1999 One-dimensional turbulence: Model formulation and application to homogeneous turbulence, shear flows, and buoyant stratified flows. *J. Fluid Mech.* **392**, 277–334.

Kerstein, A. R. 2022 Reduced numerical modeling of turbulent flow with fully resolved time advancement. Part 1. Theory and physical interpretation. *Fluids* **7** (2), 76.

Klein, M., Zenker, C. & Schmidt, H. 2019 Small-scale resolving simulations of turbulent mixing in confined jets using one-dimensional turbulence. *Chem. Eng. Sci.* **204**, 186–202.

Li, W., Yuan, M., Carter, C. D. & Tong, C. 2021 Investigation of three-scalar subgrid-scale mixing in turbulent coaxial jets. *J. Fluid Mech.* **924**, A40.

Lignell, D. O., Lansinger, V., Medina, J., Klein, M., Kerstein, A. R., Schmidt, H., Fistler, M. & Oevermann, M. 2018 One-dimensional turbulence modeling for cylindrical and spherical flows: Model formulation and application. *Theor. Comp. Fluid Dyn.* **32** (4), 495–520.

Pitsch, H. & Steiner, H. 2000 Large-eddy simulation of a turbulent piloted methane/air diffusion flame (Sandia flame D). *Phys. Fluids* **12** (10), 2541.

Rowinski, D. H. & Pope, S. B. 2013 An investigation of mixing in a three-stream turbulent jet. *Phys. Fluids* **25** (10), 105105.

Starick, T., Schmidt, H. & Lignell, D. O. 2019 One-dimensional turbulence modelling of a lifted methane/air jet flame in a vitiated coflow. *Proc. 11th Int. Symp. Turb. Shear Flow Phen. (TSFP11)* **1**, 8C, ID 278.

Walter, M., Kornev, N. & Hassel, E. 2015 Large eddy simulation of turbulent reactive mixing at high Schmidt and Reynolds numbers. *Chem. Eng. Technol.* **38** (9), 1608–1616.